Immobilization Mechanisms of Deoxyribonucleic Acid (DNA) to Hafnium Dioxide (HfO$_2$) Surfaces for Biosensing Applications

Nicholas M. Fahrenkopf,[†] P. Zachary Rice,[†] Magnus Bergkvist,[†] N. Aaron Deskins,[‡] and Nathaniel C. Cady*,[†]

[†]College of Nanoscale Science and Engineering, University at Albany, SUNY, 257 Fuller Road, Albany, New York 12203, United States

[‡]Department of Chemical Engineering, Worcester Polytechnic Institute, 100 Institute Road, Worcester, Massachusetts 01609, United States

S *Supporting Information*

ABSTRACT: Immobilization of biomolecular probes to the sensing substrate is a critical step for biosensor fabrication. In this work we investigated the phosphate-dependent, oriented immobilization of DNA to hafnium dioxide surfaces for biosensing applications. Phosphate-dependent immobilization was confirmed on a wide range of hafnium oxide surfaces; however, a second interaction mode was observed on monoclinic hafnium dioxide. On the basis of previous materials studies on these films, DNA immobilization studies, and density functional theory (DFT) modeling, we propose that this secondary interaction is between the exposed nucleobases of single stranded DNA and the surface. The lattice spacing of monoclinic hafnium dioxide matches the base-to-base pitch of DNA. Monoclinic hafnium dioxide is advantageous for nanoelectronic applications, yet because of this secondary DNA immobilization mechanism, it could impede DNA hybridization or cause nonspecific surface intereactions. Nonetheless, DNA immobilization on polycrystalline and amorphous hafnium dioxide is predominately mediated by the terminal phosphate in an oriented manner which is desirable for biosensing applications.

KEYWORDS: *deoxyribonucleic acid, DNA biosensor, hafnium dioxide, HfO$_2$, direct immobilization, phosphate*
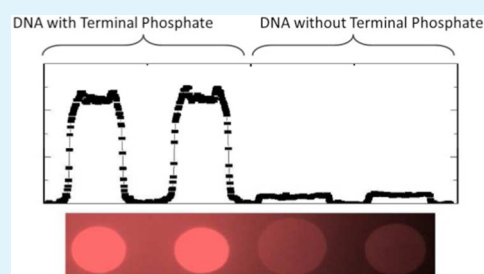
INTRODUCTION

The ability to rapidly and accurately detect DNA in field-portable devices has the potential to revolutionize pathogen detection in the health, food safety, and biowarfare arenas. DNA sensors based on field effect transistors are attractive candidates for these applications because they are small, label-free, can be highly multiplexed, and are easily fabricated with mature semiconductor processes. These sensors detect the hybridization of cDNA strands, a probe strand immobilized on the gate region of the field effect transistor (FET) and the target strand free in the sample solution. The negative charge of the DNA backbone creates an electric field in the transistor which can be measured electronically.[1−4] Over the past 15 years that FET based DNA sensors have been developed, nearly all have been fabricated with a silicon substrate and silicon dioxide as the gate dielectric.[5] In contrast, the most advanced FETs for electronics applications use hafnium dioxide as the gate dielectric because of its high dielectric constant as compared to silicon.[6] Thicker layers of hafnium dioxide can be used, yielding significantly reduced leakage current without compromising device capacitance. This is critical for integrated circuits, in which resistance/capacitance (RC) delays reduce overall processing speed.

A key technical concern for the fabrication of any DNA sensor is the immobilization of the probe strand onto the surface. This is typically accomplished with laborious surface chemical modification, including reactive silanization (for oxides) or thiol modification of so-called "noble metals" (gold, silver, etc.).[4,7−10] In both cases, the surface and/or a terminal end of the probe DNA must be chemically modified for immobilization to occur. It is well-known that FET based sensing depends on the Debye length of the sensing solution in relation to the extension of the charged analyte molecule from the substrate interface.[11−13] By directly immobilizing the probe to the gate surface, a larger portion of the charged molecule will reside within the Debye length, which should increase sensitivity of the sensor. Our group has previously shown that DNA can be tethered directly to materials commonly used in transistor manufacturing, including hafnium dioxide, through the terminal phosphate moiety of DNA strands.[14] This directional immobilization method is suitable for biosensing applications as the tethered probe is free to hybridize to target DNA. In addition, since no other surface chemistry is needed, this approach decreases the complexity of sensor fabrication and also brings the charged molecules closer to the surface. In contrast, FETs using silicon dioxide gate dielectrics require

chemical cross-linking strategies (as described above) which extend the probe DNA further from the surface of the gate. This is predicted to significantly reduce device sensitivity.[12]

In this work we further examine DNA immobilization on hafnium dioxide thin films prepared using a variety of synthesis methods and post-synthesis modification procedures. In brief, atomic layer deposited (ALD) hafnium dioxide thin films of different thickness and different anneal conditions were studied for their ability to immobilize DNA molecules with or without the terminal phosphate moiety, in both single stranded and double stranded form. In addition to the phosphate-dependent directional immobilization, a secondary immobilization mechanism was discovered and investigated. Finally, self-assembled monolayers with coordinated hafnium molecules, electron beam deposited hafnium dioxide thin films, and hafnium dioxide nanoparticles were also assessed for DNA immobilization.

■ EXPERIMENTAL SECTION

Materials. Concentrated tris-EDTA (100X TE) buffer was obtained from National Diagnostics (Atlanta, GA) and diluted 100-fold with deionized water prior to use. Sulfuric acid, hydrogen peroxide (30%), 11-mercaptoundecylphosphoric acid, 1-undecanethiol, ammonium hydroxide, 20× SSC (saline sodium citrate) buffer, poly-(α,β)-DL-aspartic acid sodium salt, and poly-L-lysine hydrobromide were obtained from Sigma-Aldrich (St. Louis, MO). Hafnium dichloride oxide octahydrate was obtained from Alfa Aesar (Ward Hill, MA). PicoGreen fluorescent dye (Invitrogen, Carlsbad, CA) was diluted into TE buffer 1:400 (v/v) prior to use. Bovine serum albumin (BSA) (New England Biolabs, Ipswich, MA) was diluted to 0.1 $\mu g/\mu L$ in TE prior to use.

Single stranded DNA oligonucleotides were purchased from Integrated DNA Technologies (Coralville, IA) having 27−29 nucleotides in length. Single stranded sequences were obtained either with ("probe-5P") or without ("probe") the 5′ terminal phosphate group, along with the complementary strand to the probes ("target"). Additional probe oligonucleotides were obtained with a Rhodamine-Red fluorescent tag on the 3′ terminus (denoted with a " * ", e.g.: probe*-5P). Finally, PolyA* and PolyT* were obtained containing 20 repeating nucleotides of adenine or thymine, respectively, and the Rhodamine-Red fluorescent tag. Upon receipt, all oligonucleotides were reconstituted to 500 μM with filter sterilized, autoclaved deionized water and stored at −20 °C.

Hafnium dioxide thin films were deposited by atomic layer deposition onto 300 mm silicon wafers and were used (I) as deposited, (II) with a postdeposition anneal, or (III) with a "deposition−anneal−deposition−anneal" process (also known as "DADA" process) described elsewhere.[15] Other hafnium dioxide films were deposited on standard glass microscope slides by reactive electron beam evaporation of metallic hafnium in oxygen at a pressure of 10^{-6} Torr.

DNA Immobilization. Prior to patterning, ALD hafnium dioxide surfaces were cleaned by immersion in piranha solution (30% H_2O_2:98% H_2SO_4, 1:2 (v/v)) for 5 min followed by a triple rinse with dH_2O before being blown dry with nitrogen gas. Single stranded probe DNA was patterned onto surfaces using a BioForce Nano eNabler[16] using 30 μm BioForce surface patterning tools (SPTs). Following printing, the samples were allowed to incubate for 12 h at room temperature. Surfaces were then triple rinsed with TE before being blocked in a solution of BSA for 20 min.[16] Samples were then triple rinsed with TE buffer and immersed in a hybridization solution of 5× SSC buffer and 100 nM target DNA. The hybridization solution was incubated at 70 °C for 5 min and allowed to cool to room temperature before being triple rinsed with TE. Hybridized samples were submerged in PicoGreen fluorescent dye. After 20 min of staining, the samples were rinsed with TE, covered with a glass coverslip, and imaged using a Nikon Eclipse 80i microscope with 490/520 nm excitation/emission. Fluorescence intensity analysis was

performed using ImageJ.[17] For each sample, the average intensity of five spots was taken, along with a background area next to each spot. The fluorescence signal for each spot was determined by normalization to the background intensity: signal = [spot intensity/background intensity] − 1. With this technique it was possible to assess DNA immobilization, spot location, and whether immobilized DNA could hybridize to the target DNA. Alternatively, if Rhodamine tagged oligonucleotides were used, they were printed as above, incubated overnight at room temperature, rinsed three times in TE, and immediately imaged using 575/605 nm excitation/emission. With this technique, it was possible to assess where DNA immobilized, without regard for the ability for the probe to hybridize.

Hafnium Terminated Self-Assembled Monolayers. Monomolecular layers of coordinated hafnium ions were prepared using self-assembled monolayer chemistry on electron beam evaporated Cr/Au samples. In 5% glacial acetic acid in ethanol 11-mercaptoundecylphosphoric acid (0.1 mM) was mixed in excess with $HfOCl_2 \cdot 8H_2O$ (5 mM) and the Au surfaces were submerged in this solution. After incubating overnight at room temperature, the surfaces were cleaned multiple times by sonication in ethanol. Thickness was monitored by variable angle spectroscopic ellipsometry (VASE), and elemental composition was assessed using X-ray photoelectron spectroscopy (XPS). VASE was performed on a JA Woollam RC2 ellipsometer. Scans were taken from 55° to 65° with 2.5° steps and then fitted to an optical model of an organic layer on a gold substrate. XPS was performed on a ThermoVG XPS Theta Probe system with an Al Kα 100W source. Survey spectra (0−1300 eV) were obtained for all samples along with higher resolution spectra of carbon (279−298 eV), nitrogen (392−410 eV), oxygen (525−545 eV), sulfur (158−172 eV), phosphorus (124−144 eV), hafnium (11−31 eV), and silicon (95−110 eV).

Hafnium Dioxide Nanoparticles. Hafnium dioxide nanoparticles were synthesized via a hydrothermal method similar to that described in ref 18. Briefly, 1.5 mL of 0.25 M $HfOCl_2 \cdot 8H_2O$ was added dropwise into 25 mL 5 M NH_4OH and then annealed at 230 °C for 3 h in a sealed reaction vessel. Once the solution cooled to room temperature, it was centrifuged and rinsed with dH_2O three times. At this point the particles were characterized with X-ray diffraction (XRD), transmission electron microcopy (TEM), and dynamic light scattering (DLS). XRD rocking curves were captured on a Bruker AXS D8 Discover diffractometer. TEM was performed on a JEOL 2010 (JEOL USA, Peabody, MA) at 200 keV. DLS was performed on a Malvern Zetasizer Nano-ZS. The mass per volume concentration of the nanoparticles was determined gravimetrically. Dilute amounts of nanoparticles were mixed with DNA and incubated in microcentrifuge tubes for 1 h after which the particles were spun down. The supernatant was analyzed at A_{260nm} using a Tecan M-200 (Durham, NC) plate reader. On the basis of standard curves, this determined the amount of DNA left in solution (from which the amount adsorbed DNA onto particles was calculated).

Simulation Methodology. Amorphous and monoclinic $[\bar{1}11]$ surfaces of hafnium dioxide were modeled at the density functional theory (DFT) level using the CP2K program.[19−21] CP2K uses a mixed basis set of Gaussian functions and plane waves. Core electrons were modeled by pseudopotentials,[22,23] while valence electrons were modeled as a double-ζ Gaussian basis set.[24] Spin-polarization was used for all calculations as well as the PBE exchange-correlation functional.[25] Periodic boundary conditions were used so that simulations of the surfaces were treated with slab models. Reciprocal space was sampled at the Γ-point. A monoclinic $[\bar{1}11]$ surface was expanded to a (2×2) supercell (13.4 Å × 14.5 Å) and was 15 Å thick. The $[\bar{1}11]$ surface has been identified as the most stable monoclinic surface.[26] The amorphous surface was cut from amorphous bulk to form a (001) surface having approximate dimensions of 16 Å x 16 Å x 11 Å. Approximately 20 Å of vacuum space was set between slabs. Illustrations of the surfaces used in the current work are shown in Figure 1. Different phosphoric acids were adsorbed on the hafnium dioxide surfaces to mimic DNA phosphate binding on the surfaces. Methyl phosphoric acid was used to mimic the terminal phosphate group of DNA, and dimethyl phosphoric acid was used to mimic the
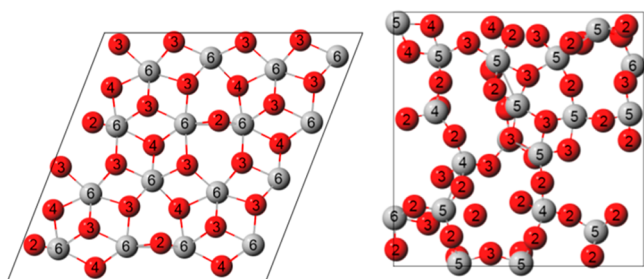
Figure 1. Top views of the monoclinic [$\bar{1}$11] (left) and amorphous [001] (right) surfaces of HfO$_2$. Numbers indicate the coordination number of the surface atoms. Gray spheres represent Hf atoms, and red spheres represent O atoms.

backbone phosphate groups of DNA. Further details on the method for generating the monoclinic and amorphous surfaces are provided in the Supporting Information.

■ RESULTS

DNA Immobilization. Hafnium dioxide can exist in a variety of crystalline and amorphous states. When hafnium dioxide is used as a high-k dielectric, a high temperature anneal is typically performed after the initial atomic layer deposition of the material. This anneal alters the crystallinity of the film, changing from amorphous to polycrystalline, in order to improve electrical characteristics. Recently, it was discovered that interspersing the annealing in between shorter ALD bursts yields films with improved electrical performance for transistor applications as compared to a single anneal after all of the ALD has been completed.[15] Our group has previously studied phosphate-dependent immobilization on unannealed hafnium dioxide. In order to study the effect of high temperature annealing on phosphate-dependent immobilization of DNA, phosphorylated and nonphosphorylated DNA was patterned onto an as-deposited (unannealed) hafnium dioxide film, as well as a hafnium dioxide film that was deposited through a deposition−anneal−deposition−anneal (DADA) process. Patterned single stranded DNA (ssDNA) probes were hybridized to cDNA target and stained with PicoGreen dsDNA stain. The resultant fluorescent intensity averages (from five spots) are shown in Figure 2. On unannealed (as-deposited) hafnium
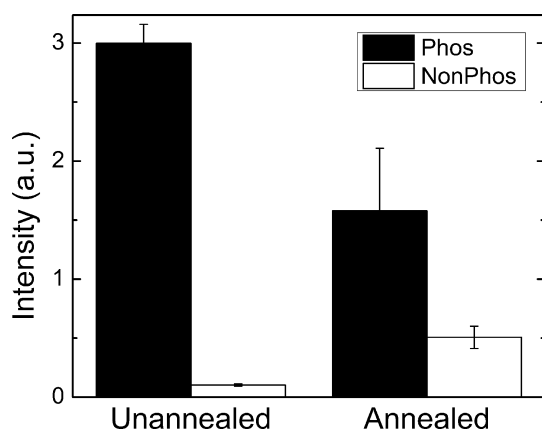
Figure 2. Dependence of DNA immobilization and hybridization on terminal phosphorylation state. Relative PicoGreen fluorescent intensity of phosphorylated (solid bars) and nonphosphorylated DNA spots after hybridization on annealed and unannaealed ALD hafnium dioxide.

dioxide, DNA immobilization and subsequent hybridization was highly dependent on the phosphorylation state of the probe DNA. For the DADA film, DNA immobilization and hybridization was less dependent on phosphorylation state, and maximum hybridization (as measured by PicoGreen fluorescence intensity) of phosphorylated DNA was reduced. However, these results may not accurately describe the relative amount of DNA that was immobilized on each hafnium dioxide surface. The PicoGreen-based fluorescence assay is a measure of the degree of DNA hybridization, not a direct measure of DNA surface immobilization. It is possible that the same amount of DNA was immobilized on each surface, but that immobilized DNA on the DADA surface was not as readily available for hybridization to target DNA.

To determine if these differences were based on the degree of probe immobilization or probe availability for hybridization, fluorescently labeled DNA probes were patterned onto the surfaces. In addition, double stranded DNA (dsDNA) solutions were prepared by mixing and heating fluorescently labeled probe DNA (phosphorylated and nonphosphorylated) with target strands and subsequently patterning onto the surfaces. These experiments enabled direct visualization of immobilized DNA, rather than relying on postimmobilization hybridization steps. The study was expanded to include two additional surfaces: a hafnium dioxide film that was subjected to a single postdeposition anneal (post dep anneal) and a 2.5 nm thick hafnium dioxide film deposited by the DADA method (as opposed to the 6.2 nm "thick" DADA film described previously). Figure 3 shows the fluorescent intensity of printed
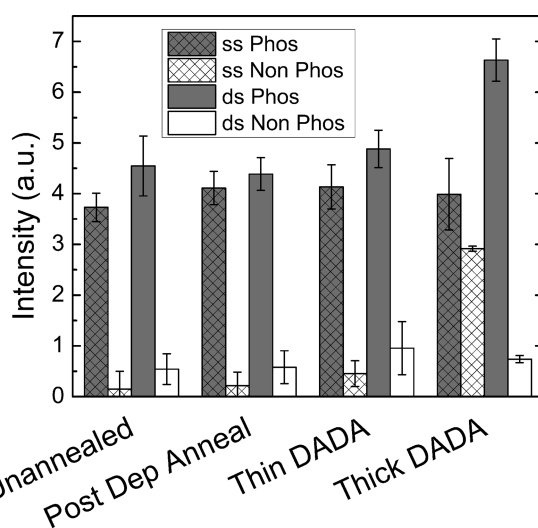
Figure 3. Relative fluorescence intensity of fluorescently labeled DNA spots on various ALD hafnium oxide surfaces. Dark bars indicate spots of phosphorylated DNA, and cross-hatching indicates single stranded DNA.

DNA spots for all four films and for all four different DNA species (single stranded and double stranded, each with or without a terminal phosphate moiety). Only the thick DADA film showed significant immobilization of single stranded, nonphosphorylated DNA. In addition, the thick DADA film showed a significantly higher amount of immobilization for phosphorylated dsDNA. For the other three films, only immobilization of phosphorylated DNA was observed. These data support our previous hybridization-based results, which suggested that phosphorylation state of the DNA probe was
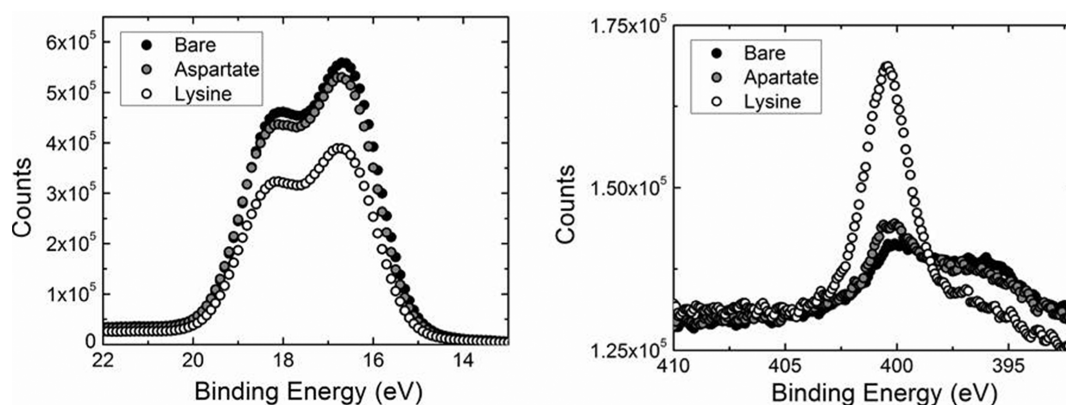
Figure 4. X-ray photoelectron spectroscopy scans of the Hf 4f (left) and N 1s (right) regions. Solid black markers represent the bare hafnium dioxide substrate, gray markers are the hafnium dioxide patterned with poly aspartate, and white markers are the hafnium dioxide patterned with poly lysine.

critical for immobilization. In addition, significantly more nonphosphorylated ssDNA was immobilized on thick DADA films than on other three films. On the basis of our hybridization results in Figure 2, there was also less hybridization of complementary target on the thick DADA surfaces. This suggests that a secondary interaction mechanism may occur on these substrates, which reduces the availability of probe DNA for hybridization.

The dominant electrochemical property of the DNA backbone is negative charge, which stems from multiple phosphate groups (one phosphate per nucleotide). The limited amount of nonphosphorylated dsDNA immobilization observed on all hafnium dioxide surfaces suggests that there are limited interactions between the sugar−phosphate DNA backbone and hafnium dioxide. Thus, we hypothesized that negative electrostatic charge based interactions play a small role in DNA attachment to hafnium dioxide. To further investigate this hypothesis, two model polyelectrolytes were deposited onto hafnium dioxide surfaces and their immobilization status was evaluated. Poly aspartic acid (poly aspartate) was chosen as a negatively charged polyelectrolyte, while poly lysine was chosen as a positively charged polyelectrolyte. At neutral pH, the carboxylate-terminated side-chains of poly aspartate are deprotonated, yielding a net negative charge, while the amino-terminated side-chains of poly lysine are protonated, yielding a net positive charge. Solutions of these polyelectrolytes were spotted onto thick DADA films using a micropipet, incubated overnight at room temperature, washed repeatedly with deionized water, and then analyzed with XPS (Figure 4).

The Hf 4f signal was monitored to determine if polyelectrolyte was covering the hafnium dioxide surface (thereby blocking the Hf 4f signal), while the N 1s signal was monitored to directly determine the presence or absence of polyelectrolyte. The results shown in Figure 4 indicate that poly lysine was immobilized on the thick DADA surface, as demonstrated by a reduction in Hf 4f signal, and an increase in N 1s signal (as compared to the bare hafnium dioxide film). The poly aspartate patterned sample yielded results similar to the bare hafnium dioxide, suggesting that this polyelectrolyte did not bind in any significant amount. Combined, these results suggest that positively charged polyelectrolytes adsorb through electrostatic interactions on thick DADA surfaces. It further suggests that the thick DADA substrates have a net negative surface charge, which supports our hypothesis that the

negatively charged backbone of DNA does not significantly contribute to its attachment to this surface. On the basis of these findings, we suggest that the exposed nucleotide bases of ssDNA can interact with the thick DADA surface and contribute to surface attachment.

It has been previously demonstrated that individual purine bases can coordinate to transition metal oxides (including titanium oxide).[27−30] To investigate the specific binding of purines in our system, fluorescently labeled, twenty base oligonucleotides of adenine (PolyA*) and of thymine (PolyT*) were patterned onto unannealed ALD hafnium dioxide and the thick DADA hafnium dioxide. As shown in Figure 5, PolyT*
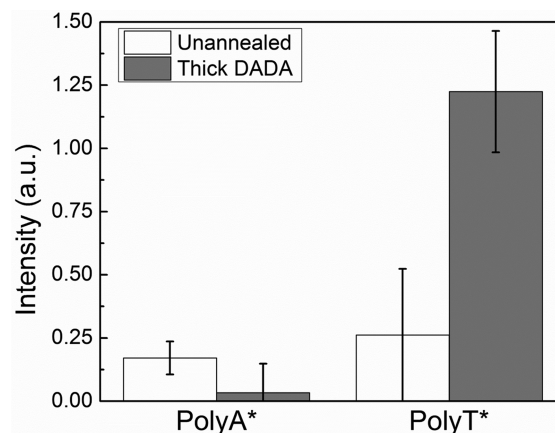
Figure 5. Relative fluorescence intensity of fluorescently labeled nonphosphorylated poly adenine and poly thymine on unannealed (open bars) and thick DADA (solid bars) hafnium dioxide.

immobilized significantly more that PolyA*, and only on the thick DADA film. These ssDNA oligonulceotides did not have the terminal phosphate moiety, so any immobilization was predicted to be mediated by the secondary immobilization method. In contrast to other reports, in our study the pyrimidine (PolyT*) appears to bind, not the purine (PolyA*).

Simulation of DNA Surface Interactions. To further investigate the interactions of different phosphate groups with hafnium dioxide surfaces, we modeled methyl phosphoric acid and dimethyl phosphoric acid adsorption over amorphous and monoclinic surfaces. The amorphous [001] surface represented the unannealed surface, while the monoclinic [$\bar{1}$11] represented

the DADA surface.[31] Methyl phosphoric acid mimics the structure of a terminal phosphate group (before hydrogen removal) in DNA, while dimethyl phosphoric acid mimics the structure of a backbone phosphate group in DNA. We considered dissociated and undissociated adsorption of the phosphoric acids, but dissociation of all or some of the −OH groups was preferred. Dissociated phosphoric acid represents a phosphate group and is a model representation of a phosphate group from DNA. We also tried a variety of initial phosphoric acid coordination geometries (e.g., bidentate with two Hf−O bonds, or tridentate with three Hf−O bonds). We modeled adsorption modes and a summary of the most stable geometries are given in Table 1. The most relevant adsorption modes for

Table 1. Calculated Adsorption Energies of Different Phosphoric Acids over the Amorphous and Monoclinic Surfaces from a Variety of Initial Configurations[a]

molecule adsorbed/surface	adsorption energy (kJ/mol)	binding mode
methyl phosphoric acid/amorphous [001]	−258	tridentate
	−231	bidentate
	−205	bidentate
	−151	bidentate
methyl phosphoric acid/monoclinic [$\bar{1}$11]	−314	bidentate
	−285	bidentate
	−272	tridentate
	−243	bidentate
dimethyl phosphoric acid/amorphous [001]	−192	bidentate
	−190	bidentate
	−168	bidentate
dimethyl phosphoric acid/monoclinic [$\bar{1}$11]	−278	bidentate
	−244	bidentate
	−217	bidentate

[a]More negative adsorption energies indicate more exothermic (more favorable) binding.

methyl phosphoric acid are also illustrated in Figure 6. In general, the binding of the methyl phosphoric acid to either surface was more favorable than the dimethyl phosphoric acid, and binding on monoclinic hafnium dioxide was more stable than the amorphous surface. The only stable geometry for dimethyl phosphoric acid was bidentate binding, while the methyl phosphoric acid exhibited binding with bidentate and tridentate geometries.
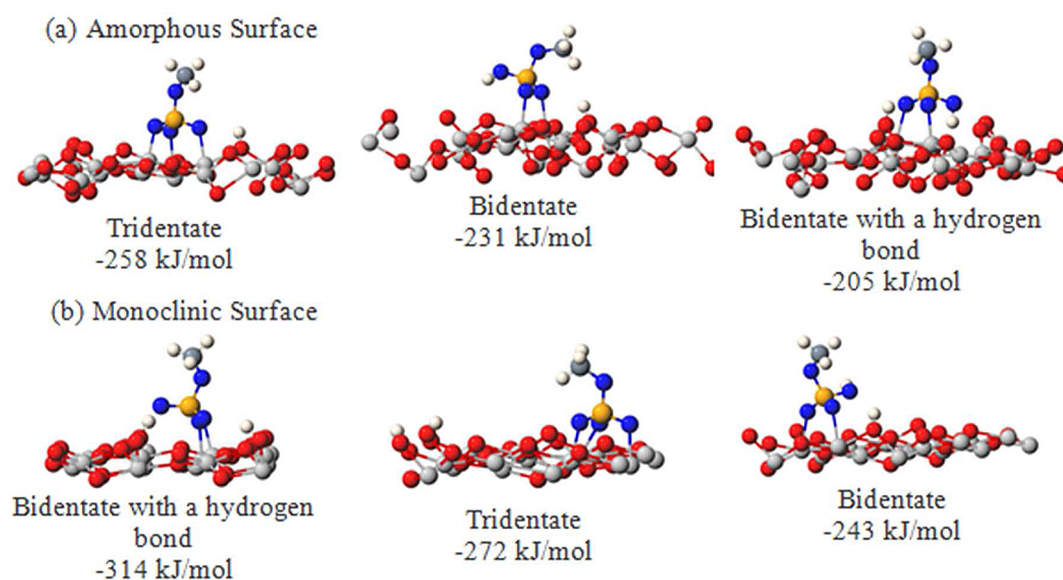
Hafnium Dioxide Film Characterization. To understand how our modeling results relate to our fluorescence data, we analyzed published data on the surfaces used. Grazing incident small-angle X-ray scattering (GIAXS), X-ray photoelectron spectroscopy (XPS), ultraviolet photoelectron spectroscopty (UPS), and spectroscopic ellipsometry (SE) measurements have been previously performed on the hafnium dioxide films used in this study.[32] These studies showed that the thick DADA film is the only film with a clear monoclinic crystal structure. The other films (postdeposition annealed, unannealed, and thin DADA) were either amorphous or a mixed phase of monoclinic, tetragonal, and/or orthorhombic phases. Since the thick DADA was the only film to which nonphosphorylated ssDNA was immobilized, our proposed nucleobase-dependent attachment may depend on a monoclinic crystal structure.

Evaporated and Self-assembled Monolayer Deposited Films. To further explore phosphate-dependent DNA immobilization on hafnium-based surfaces, we studied self-assembled monolayers (SAMs) containing hafnium ions and hafnium dioxide deposited by oxygen reactive electron beam evaporation (as opposed to the atomic layer deposition based films used above). Neither of these surfaces was expected to be crystalline, and therefore, we hypothesized that DNA immobilization would be governed by the presence or absence of a terminal phosphate moiety. The immobilization of fluorescently labeled ssDNA onto these surfaces (Figure 7) is similar to that seen on unannealed (amorphous) hafnium dioxide (from Figure 3). This suggests that SAMs with coordinated hafnium ions and evaporated hafnium dioxide may both be suitable surfaces for other DNA immobilization

Figure 6. Illustration of DFT adsorption geometries for methyl phosphoric acid over the (a) amorphous and (b) monoclinic surfaces. Light gray spheres represent Hf atoms, red spheres represent O atoms of the surface, white spheres represent H atoms, dark gray spheres represent C atoms, orange atoms represent P atoms, and blue spheres represent O atoms of the phosphoric acid.
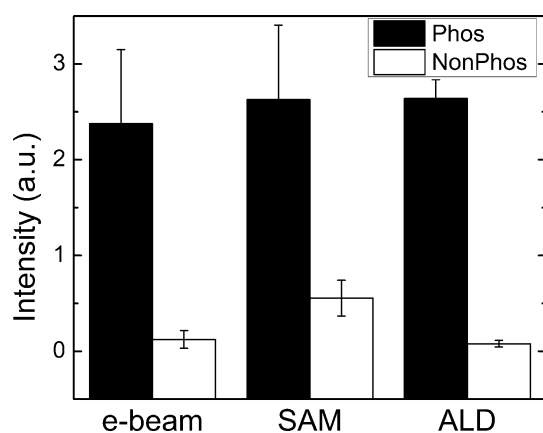
Figure 7. Relative fluorescence intensity of fluorescently labeled phosphorylated (solid bars) and nonphosphorylated DNA spots on hafnium-containing surfaces: e-beam evaporated hafnium oxide (e-beam), self-assembled monolayers of hafnium ion (SAM), and unannealed atomic layer deposition of hafnium oxide (ALD).

and biosensing applications. While not practical for FET based DNA sensing, these surface preparations may be useful for applications where ALD hafnium dioxide is not practical or available. SAMs can be fabricated in any laboratory with wet chemical capabilities, and evaporative hafnium dioxide is much more readily available than ALD-deposited material.

Hafnium Dioxide Nanoparticles. In addition to planar electrical detection devices, biosensors based upon nanoparticle reporters/substrates are currently being developed.[33,34] To demonstrate the utility of DNA−hafnium dioxide interactions for such devices, we explored immobilization of DNA on hafnium dioxide nanoparticles. The left side of Figure 8 shows the ability of ssDNA immobilization onto chemically synthesized hafnium dioxide nanoparticles. As the inset shows, at lower concentrations of DNA the phosphorylated DNA immobilizes to a higher degree than nonphosphorylated DNA. At higher concentrations of DNA, however, nonphosphorylated DNA is immobilized to a much greater extent than phosphorylated DNA.

The observation that nonphosphorylated ssDNA adsorbed on to hafnium dioxide nanoparticles is similar to our results for thick DADA substrates, which were negatively charged and with a monoclinic crystal structure. Characterization by electron microscopy, X-ray diffraction, and zeta potential (Figure 8, right) demonstrated that our nanoparticles have similar properties (20−40 nm diameter, monoclinic, negative surface charge) as the thick DADA substrates.

■ DISCUSSION

It has been demonstrated that phosphate functional groups of various organic molecules can coordinate to metal oxides, including hafnium dioxide.[35] This phosphate coordination chemistry could be exploited for oriented surface attachment of DNA for biosensing applications, provided that surface immobilization does not interfere with hybridization. In this study, we investigated the influence of terminal phosphate groups present on DNA upon binding to various hafnium dioxide substrates. We demonstrated successful hybridization by fluorescently staining immobilized DNA after exposure to complementary target DNA. Analysis of differentially prepared hafnium dioxide surfaces (annealed and unannealed) revealed that DNA immobilization and hybridization is influenced by the phosphorylation state of the DNA as well as the nature of the hafnium dioxide film. Analysis using fluorophore-labeled DNA aimed to further characterize the nature of the DNA−surface interaction on various interfaces. Figure 3 shows that nonphosphorylated ssDNA immobilizes to the thick DADA hafnium dioxide surface nearly as well as the phosphorylated ssDNA. The fluorescence intensity of the nonphosphorylated DNA spots was at least 75% as bright as the intensity of the phosphorylated DNA spots. In comparison, in Figure 2, the intensity of the nonphosphorylated DNA spots after hybridization was less than half as intense as the phosphorylated spots. These results suggest that some amount of ssDNA immobilized to the surface of the thick DADA hafnium dioxide was not able to hybridize. In addition, Figure 3 shows that immobilization was dependent on the hybridization state (single or double stranded) of the DNA, its phosphorylation state, and the surface properties of the hafnium dioxide film. In particular, we noted that single stranded, nonphosphorylated DNA bound to hafnium dioxide with monoclinic crystal structure, but much less to amorphous or mixed crystallinity interfaces. These results indicated that multiple interactions are
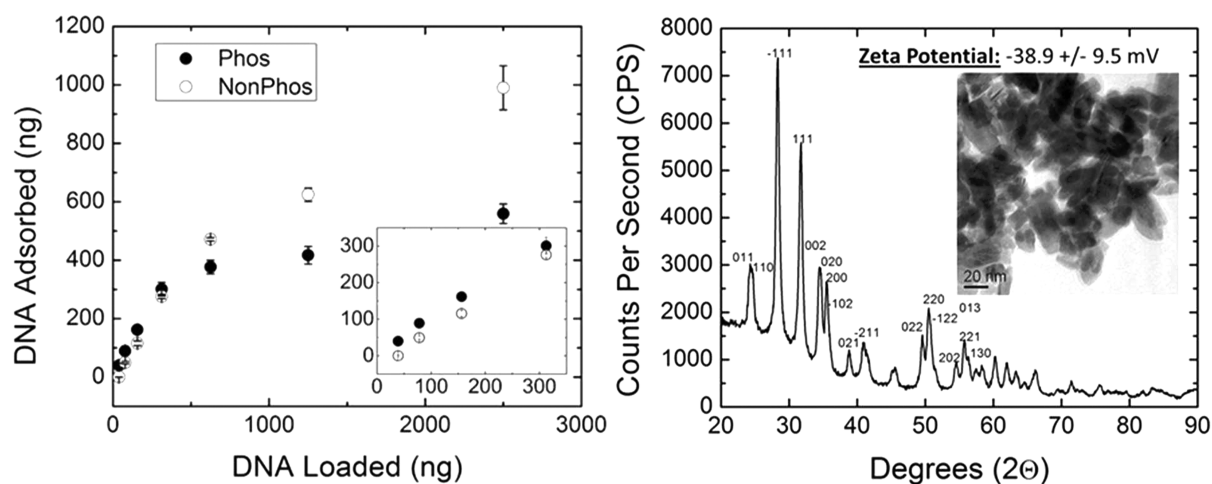
Figure 8. (left) Adsorption of phosphorylated and nonphosphorylated ssDNA on hafnium oxide nanoparticles. (right) Characterization of hafnium oxide nanoparticles including XRD peak identification of monoclinic peaks, TEM micrograph, and zeta potential of the surface of the particles.

involved in ssDNA adsorption to monoclinic hafnium dioxide. One interaction is likely the coordination of the terminal phosphate moiety with the hafnium dioxide surface. Other possible modalities include binding via exposed nucleobases or electrostatic interaction through the phosphate backbone. Further studies (below) show that electrostatic interaction is not occurring.

Our DFT simulations (Table 1 and Figure 6) of phosphoric acid binding indicate that both methyl phosphoric acid (a model for the terminal phosphate moiety in phosphorylated DNA) and dimethyl phosphoric acid (a model for a backbone phosphate group in DNA) preferentially bind to the monoclinic $[\bar{1}11]$ surface over the amorphous $[001]$ surface. As Figure 6 illustrates in the case of methyl phosphoric acid, a variety of binding modes are possible, with bidentate and tridentate interactions the most stable. Dimethyl phosphoric acid prefers bidentate adsorption. The key to strong bonding of the phosphate is the ability of several Hf atoms to interact with the O atoms of the phosphate. Several bidentate interactions are possible whereby an OH group of the phosphate interacts with a surface O atom (Figure 6b, left). The amorphous surface is dominated by a number of uncoordinated Hf atoms (four- and five-coordination), while Hf prefers six-coordination as shown in Figure 1. In contrast, the Hf atoms of the monoclinic surface are all six-coordinated. One may thus presume that the amorphous surface will bind molecules more strongly to the surface in order for surface atoms to reach the optimal bonding configuration. This, however, is not the case as our calculations show. The amorphous surface atoms are not arranged in an ordered fashion, so the Hf atoms have difficulty obtaining the ordered octahedral geometry of bulk hafnium dioxide, thus surface bonding can be strained. Furthermore, bidentate or tridentate bonding of the phosphoric acid requires two or three Hf atoms of the appropriate distance and geometry to accommodate Hf−O bonding. The regular structure of the monoclinic $(\bar{1}11)$ surface allows a phosphate to bind to several nearby Hf atoms and form the appropriate binding complex. The disordered structure of the amorphous surface, however, prevents a phosphate from interacting with the required Hf atoms in an optimal fashion.

Our calculations (Table 1) show that dimethyl phosphoric acid binds less strongly to the surfaces than methyl phosphoric acid. Assuming that dissociated dimethyl phosphoric acid is a reasonable model of a backbone phosphate group, this agrees with our premise that phosphorylated DNA binds stronger to hafnium dioxide than nonphosphorylated DNA. Assuming also that dissociated phosphoric acid is a reasonable model of a terminal phosphate group, our calculations show that phosphorylated DNA prefers DADA (monoclinic) over unannealed (amorphous) hafnium dioxide, and we also show that nonphosphorylated DNA prefers DADA (monoclinic) over unannealed (amorphous). However, we must acknowledge that our model is rather simplistic, in that we ignore the DNA nucleotides and steric hindrance of the DNA molecule, as well as aqueous environment; however, the calculations do support the notion of phosphate groups binding stronger to the DADA (monoclinic) surfaces compared to unannealed (amorphous) surfaces and that phosphorylated DNA binds stronger than nonphosphorylated DNA.

When investigating surface attachment behavior, we must consider the importance of surface charge and the electrostatic properties of the DNA molecule. The observation that nonphosphorylated ssDNA did adsorb to thick DADA films, while nonphosphorylated dsDNA did not, suggests that backbone phosphates may have little effect on the binding. To further evaluate the electrostatic interactions on thick DADA hafnium dioxide, we studied the adsorption of two polyelectrolytes. The results of these experiments strongly suggest that the surface of the thick DADA is negatively charged, evidenced by the observation that positively charged poly lysine immobilized to a greater degree than negatively charged poly aspartate). These results further suggest that immobilization of nonphosphorylated DNA is not due to backbone−surface interactions. We suggest instead that beyond the terminal phosphate interaction, surface immobilization may be mitigated by exposed nucleotide bases of ssDNA, where the amine bases could form Lewis acid−base coordination bonds with the hafnium dioxide. In support of this hypothesis, we showed that nonphosphorylated dsDNA attached poorly to thick DADA interfaces (Figure 3), which is to be expected since the bases would have little interaction with the surface in dsDNA.

While no detailed studies have been performed on nucleobase interactions with hafnium dioxide, it has been shown through computational and NMR studies that a wide range of metal ions, including titanium, will bind to nucleobases, primarily through the N7 purines.[27−29] Most recently, Monti and Walsh performed computational studies of nucleobases on a titanium oxide crystal surface with similar results.[30] We hypothesized that the "non-phosphate" interactions between ssDNA-hafnium dioxide were similar since titanium and hafnium are similar transition metal oxides. However, in our experiments the pyrimidine (thymine) oligonucleotide immobilized to the monoclinic hafnium dioxide, but not the purine (adenine). It should be noted that the experimental evidence of purines binding to metal oxides are for single nucleotides and metal ions, not for oligonucleotides on a two-dimensional surface, such as were used in the present study. Therefore, the mechanism for thymine binding to the hafnium dioxide surface over adenine warrants further investigation and should be investigated in conjunction with cytosine and guanine immobilization.

The monoclinic hafnium dioxide DADA thin films were unique in their binding to both phosphorylated and nonphosphorylated ssDNA. Other groups have studied these thick DADA films for nanoelectronics applications and have found improvements in the equivalent oxide thickness for this type of surface.[15] However, since the focus of those studies was on the electronic properties of the film, the surface properties of the film were not reported. Bersch et al. investigated various ALD deposited hafnium dioxides with multiple techniques; while most of their analyses support the monoclinic nature of the thick DADA films, they noted an absence of the $[-111]$ peak which should have been present for this phase.[32] They hypothesized that this could be due to a fiber texture of the film. Recently, Consiglio, et al. confirmed this texture using pole figure measurements, which proved that the thick DADA film has a highly ordered continuous monoclinic crystal structure with the $[-111]$ crystal face at the surface.[31] The theoretical crystal spacing of $[-111]$ hafnium dioxide is 3.6 Å, and TEM measurements of the thick DADA films showed a lattice parameter closer to 3.1 Å. Coincidentally, this range of crystal spacing for the $[-111]$ face spans the length of a single nucleotide (3.4 Å) in the dsDNA molecule.[36] Further, recent simulations of ssDNA near various surfaces have shown that the length of a nucleotide can range from 2.8 to 3.7 Å.[37] The top

5366

dx.doi.org/10.1021/am3013032 | ACS Appl. Mater. Interfaces 2012, 4, 5360−5368

down TEM of the DADA film showed a very smooth and uniform morphology, while unannealed and PDA hafnium dioxide have more surface inhomogeneities.

In addition to ALD hafnium dioxide, DNA immobilization onto other forms of hafnium was studied including nanoparticles, physical vapor deposited hafnium dioxide thin films and self-assembled monolayers. Similar to the thick DADA hafnium dioxide film, the hafnium dioxide nanoparticles studied here were monoclinic in crystal structure with a negative surface charge (as determined by zeta-potential measurements). The particles exhibited similar ability to immobilize both phosphorylated and nonphosphorylated DNA as the thick DADA film; however, further study is needed to understand immobilization behavior at higher concentrations of DNA. Specifically, more study is needed to understand why phosphorylated DNA immobilization appears to plateau at moderate DNA loading concentrations while nonphosphorylated immobilization steadily increases. In contrast, the thin film of hafnium dioxide deposited by electron beam evaporation and the self-assembled monolayers are not expected to be monoclinic in nature, and therefore, we hypothesized that DNA immobilization would be dominated by the directional terminal phosphate-dependent immobilization. The data in Figure 7 show that phosphorylated ssDNA immobilized to these two forms of hafnium in a similar ratio as the previously studied unannealed ALD hafnium dioxide; therefore, these forms of hafnium dioxide could also be used in biosensing applications which require a directional immobilization. While there are differences between monoclinic hafnium dioxide and all other hafnium dioxide surfaces studied here, all the surfaces studied do immobilize DNA.

CONCLUSIONS

In this work we have expanded studies on the phosphate-dependent oriented immobilization of DNA to hafnium dioxide. While a phosphate specific immobilization is observed on many different types of hafnium dioxide surfaces, we observed a second interaction mode on monoclinic hafnium dioxide. We propose that this interaction stems from exposed nucleobases in ssDNA aligned with the repeating atomic structure of smooth, crystalline hafnium dioxide that has a lattice spacing that matches the base-to-base pitch in DNA. This second interaction mechanism would not be ideal for biosensing applications, since the bases are not available for hybridization. Further, we note that more amorphous hafnium dioxide films exhibit only the phosphate-dependent immobilization.

ASSOCIATED CONTENT

ⓢ Supporting Information

Details on the generation of the surfaces used here in the DFT modeling. This information is available free of charge via the Internet at http://pubs.acs.org.

AUTHOR INFORMATION

Corresponding Author
*E-mail: ncady@albany.edu.

Notes

The authors declare no competing financial interest.

ACKNOWLEDGMENTS

REFERENCES

(1) Souteyrand, E.; Cloarec, J. P.; Martin, J. R.; Wilson, C.; Lawrence, I.; Mikkelsen, S.; Lawrence, M. F. *J. Phys. Chem. B* **1997**, *101*, 2980−2985.

(2) Gonçalves, D.; Prazeres, D. M. F.; Chu, V.; Conde, J. P. *Biosens. Bioelectron.* **2008**, *24*, 545−551.

(3) Ishige, Y.; Shimoda, M.; Kamahori, M. *Jpn. J. Appl. Phys.* **2006**, *45*, 3776−3783.

(4) Sakata, T.; Miyahara, Y. *Biosens. Bioelectron.* **2005**, *21*, 827−832.

(5) Grieshaber, D.; MacKenzie, R.; Vörös, J.; Reimhult, E. *Sensors* **2008**, *8*, 1400−1458.

(6) Robertson, J. *J. Appl. Phys.* **2008**, *104*, 124111.

(7) Su, M.; Li, S.; Dravid, V. P. *Appl. Phys. Lett.* **2003**, *82*, 3562−3564.

(8) Hur, Y.; Han, J.; Seon, J.; Pak, Y. E.; Roh, Y. *Sens. Actuators, A* **2005**, *120*, 462−467.

(9) Wang, R.; Tombelli, S.; Minunni, M.; Spiriti, M. M.; Mascini, M. *Biosens. Bioelectron.* **2004**, *20*, 967−974.

(10) Ganguly, A.; Chen, C.-P.; Lai, Y.-T.; Kuo, C.-C.; Hsu, C.-W.; Chen, K.-H.; Chen, L.-C. *J. Mater. Chem.* **2009**, *19*, 928−933.

(11) Nair, P. R.; Alam, M. A. *IEEE Trans. Electron Devices* **2007**, *54*, 3400−3408.

(12) Stern, E.; Wagner, R.; Sigworth, F. J.; Breaker, R.; Fahmy, T. M.; Reed, M. A. *Nano Lett.* **2007**, *7*, 3405−3409.

(13) Balasubramanian, K. *Biosens. Bioelectron.* **2010**, *26*, 1195−1204.

(14) Fahrenkopf, N. M.; Shahedipour-Sandvik, F.; Tokranova, N.; Bergkvist, M.; Cady, N. C. *J. Biotechnol.* **2010**, *150*, 312−314.

(15) Clark, R. D.; Aoyama, S.; Consiglio, S.; Nakamura, G.; Leusink, G. *ECS Trans.* **2011**, *35*, 815−834.

(16) Xu, X.; Jindal, V.; Shahedipour-Sandvik, F.; Bergkvist, M.; Cady, N. C. *Appl. Surf. Sci.* **2009**, *255*, 5905−5909.

(17) Abramoff, M. D.; Magalhaes, P. J.; Ram, S. J. *Biophoton. Int.* **2004**, *11*, 36−42.

(18) Meskin, P. E.; Sharikov, F. Y.; Ivanov, V. K.; Churagulov, B. R.; Tretyakov, Y. D. *Mater. Chem. Phys.* **2007**, *104*, 439−443.

(19) CP2K developers homepage. http://www.cp2k.org/ (accessed June 15th, 2012).

(20) Lippert, G.; Hutter, J.; Parrinello, M. *Theor. Chem. Acc.* **1999**, *103*, 124−140.

(21) VandeVondele, J.; Krack, M.; Mohamed, F.; Parrinello, M.; Chassaing, T.; Hutter, J. *Comput. Phys. Commun.* **2005**, *167*, 103−128.

(22) Krack, M. *Theor. Chem. Acc.* **2005**, *114*, 145−152.

(23) Goedecker, S.; Teter, M.; Hutter, J. *Phys. Rev. B: Condens. Matter Mater. Phys.* **1996**, *54*, 1703−1710.

(24) VandeVondele, J.; Hutter, J. *J. Chem. Phys.* **2007**, *127*, 114105.

(25) Perdew, J. P.; Burke, K.; Ernzerhof, M. *Phys. Rev. Lett.* **1996**, *77*, 3865−3868.

(26) Mukhopadhyay, A.; Sanz, J.; Musgrave, C. *Phys. Rev. B: Condens. Matter Mater. Phys.* **2006**, *73*, 115330.

(27) Robertazzi, A.; Platts, J. *JBIC, J. Biol. Inorg. Chem.* **2005**, *10*, 854−866.

(28) Froystein, N. A.; Sletten, E. *Acta Chem. Scand.* **1991**, *45*, 219−225.

(29) Noguera, M.; Branchadell, V.; Constantino, E.; Ríos-Font, R.; Sodupe, M.; Rodríguez-Santiago, L. *J. Phys. Chem. A* **2007**, *111*, 9823−9829.

(30) Monti, S.; Walsh, T. R. *J. Phys. Chem. C* **2011**, *115*, 24238−24246.

(31) Consiglio, S.; Clark, R. D.; Bersch, E.; LaRose, J.; Wells, I.; Tapily, K.; Leusink, G. J.; Diebold, A. *ECS Trans.* **2011**, *41*, 89−108.

(32) Bersch, E.; LaRose, J. D.; Wells, I.; Consiglio, S.; Clark, R. D.; Leusink, G. J.; Matyi, R. J.; Diebold, A. C.; Seiler, D. G.; Diebold, A. C.; McDonald, R.; Chabli, A.; Secula, E. M. *AIP Conf. Proc.* **2011**, *1395*, 154−160.

(33) Sanvicens, N.; Pastells, C.; Pascual, N.; Marco, M.-P. *TrAC, Trends Anal. Chem.* **2009**, *28*, 1243−1252.

(34) Pedroso, S.; Guillen, I. A. *Comb. Chem. High Throughput Screening* **2006**, *9*, 389−397.

(35) Jespersen, M. L.; Inman, C. E.; Kearns, G. J.; Foster, E. W.; Hutchison, J. E. *J. Am. Chem. Soc.* **2007**, *129*, 2803−2807.

(36) Watson, J. D.; Crick, F. H. C. *Nature* **1953**, *171*, 737−738.

(37) Ambia-Garridoa, J.; Vainrubb, A; Montgomery Pettitt, B. *Comput. Phys. Commun.* **2010**, *181*, 2001−2007.